Available online at www.sciencedirect.com

Science Direct

materialstoday: PROCEEDINGS

[International Conference on Energy and Environment (iCEE 2k19)]

Hesperidin mediated synthesis, structure and optical emission analysis on nanocrystalline CuO

Praveen K. H.[1] and Arun S. Prasad[2]*

[1]*Post Graduate Department of Physics, S. N. College, Chengannur, Alappuzha-689508, Kerala, India*
[2]*Post Graduate Department of Physics, TKMM College, Nangiarkulangara, Alappuzha-690513, Kerala, India*
**Corresponding author, email: asp.physics@gmail.com*

Abstract

Nanocrystalline Copper (II) oxide was synthesized through hesperidin mediated phytochemical reduction method and post annealed at 600 ^{o}C for 4 hrs. Various analytical results obtained after characteristic measurements such as XRD, FESEM, UV-visible spectroscopy and Photoluminescence studies have been discussed. The crystallographic plane reflections obtained in X-ray diffraction pattern was found to be analogous with the monoclinic end centered phase of copper (II) oxide with Halder-Wagner crystallite size 18 nm. The formation of spherical grains via agglomerated crystallites was apparent from the surface morphology obtained through FESEM images. Tauc' plot of UV-visible spectrum employing Kubelka-Munk function provided a direct optical band gap of 1.61 eV. The photoluminescence spectrum using 280 nm optimal excitation wavelength and the related CIE plot revealed that the optical emission occurs at blue region as indicated by the chromaticity coordinates.

Keywords: Hesperidin, nanocrystalline, photoluminescence, optical band gap, chromaticity etc;

1. Introduction

Metal oxide nanoparticles are the widely interested candidates in the contemporary research on materials syntheses, crystallography and optical emission studies. Simple transition metal oxides with high quality crystalline behavior have been established as direct band gap materials [1-3] and hence being considered as appropriate candidates for optoelectronic device applications. At present, the complex alloying of III/V or IV/VI group elements with appropriate doping technique is commercially used for making direct band gap materials [4]. This is often cumbersome that the band gap tuning remains difficult in such materials. The advent of direct band gap behavior in simple transition metal oxides opened up much attention towards their applications in optoelectronic device applications. Interestingly, the nanocrystalline regime in such oxides could further incorporate the tuning behavior in the band gap by varying the crystallite size. Among simple metal oxides, copper (II) oxides are widely explored due to their combined electrical, optical and magnetic properties [5, 6]. Many number of studies have been reported elsewhere related to the syntheses, crystallographic structure and optical analyses on nanocrystalline CuO through various synthesis techniques such as inter diffusion process [7], hydrothermal route [8], vapour phase approach [9], sonochemical method [10], microwave assisted hydrothermal method [11], phytochemical mediated synthesis [3,12] etc. Among these, phytochemical mediated synthesis technique is comparatively novel and less expensive [13].

.

However, one of the major tribulations with this green approach is the difficulties in separating the exact phytochemical reductant from the mixture of plant extract, which often leads to poor yield of high quality crystalline products. In order to overcome this crisis, a high purity phytochemical, namely hesperidin, capable of acting as effective reductants were utilized to directly substitute for complex plant extracts.

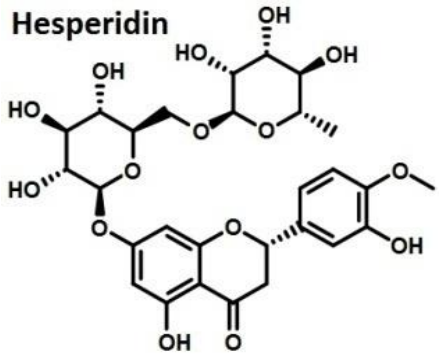

Fig.1. Structure of Hesperidin (EPA substance registry system: Hesperidin (520-26-3))

Hesperidin is a bioflavonoid, which was first separated in 1828 from the inner section of orange peels [14]. Profuse quantity of Hesperidin is found in citrus fruits such as orange, lemon, grapes etc. Depending on species, parts, geographic sites of cultivation and processing procedures, the content of hesperidin varies greatly in citrus fruits [14]. In this context, this paper disuses the characteristic studies on CuO nanocrystallites synthesized through commercially available hesperidin as phytochemical mediator.

2. Experimental

Aqueous solution of 0.1 M $CuSO_4.5H_2O$ precursor salt mixed with 0.0125 M alkaline solution of hesperidin (purchased from Sigma Aldrich) dissolved in 1M NaOH solution by keeping 2:3 volume ratio. The mixture was allowed to react at room temperature for 1 hr under constant stirring and pH of the reaction mixture was regularly tested and maintained at 7 to 8. The deep change in color during the course of reaction was indicative of the reduction reaction being carried out. The mixture was then kept in dark for an overnight settle down, and the solid residues obtained was separated using whatman filter paper. The filtrate was then washed several times using de-ionized water to remove the adhering impurity contents and then dried in air. The crushed fine powder of the sample was then kept in crucible for annealing at 600 ^oC for 4 hrs. The sample is here after referred to as Cu-NP-HESPN. Various analytical results obtained after characteristic measurements such as XRD, FESEM, UV-visible spectroscopy and Photoluminescence studies have been discussed.

The possible mechanism involves the reduction of precursor salt, yielding copper oxide nanoparticles with complex sterric encasing with hesperidin. The hydroxyl groups present in hesperidin is capable of having larger binding affinity with the metallic copper ions present in the precursor salt. This results in the reduction of the salt and there by the copper ions are moved to attach with hydroxyl groups present in hesperidin. Depending on the reaction temperature and pH, the copper ions further undergo oxidation process and copper oxide nanoparticles are released with surface sterric stability against agglomeration. The addition of NaOH expedites the removal of copper ions from precursor salt. Since the hydroxyl group present in the hesperidin is compared to have larger affinity to bind with copper ions, the NaOH remains acted as catalyst alone

3. Results and discussion

3.1. X-ray diffraction pattern analysis

The X-ray diffraction pattern recorded in BRUKER D8 ADVANCE diffractometer system with 280 goniometer radius was used to study the crystallographic features and crystallite size dimension of the sample. Figure 2 depicts the X-ray diffraction pattern resulted for 600 ^oC annealed powder sample, Cu-NP-HESPN. An X-ray wavelength of 1.5406 Å was allowed to pitch on the sample in scan angle, 2θ ranging from 10° to 90° in 0.020348 step size [15]. The observed Bragg reflection peaks were indexed with crystallographic plane reflections analogous to the monoclinic end centered phase of copper (II) oxide (CuO) as reported in JCPDS: ICDD PCPDFWIN #PDF Number: 89-5895 under the space group C2/c (15). The pattern lacks any un-indexed peaks, implying the absence of any additional phases or

impurity content, and hence apparently evidenced the formation of purely single phase crystallites of monoclinic end centered crystallites of CuO.

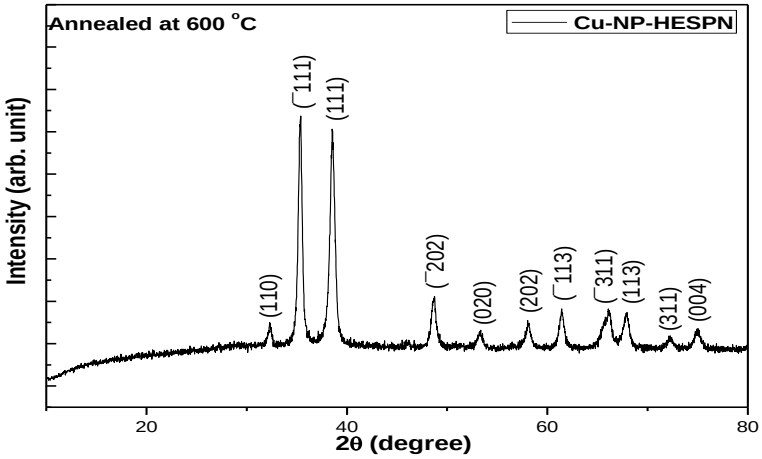

Fig. 2. XRD pattern Cu-NP-HESPN sample

Considerable extent of broadening in the X-ray reflection peaks indicates the formation of nano-dimensional regime in crystal structure. The crystallite size and strain were estimated through Halder-Wagner method [16]:

$$\left(\frac{\beta^*}{d^*}\right)^2 = \frac{K\beta^*}{D_{H-W}(d^*)^2} + (2\varepsilon_{H-W})^2 \qquad (1)$$

where β^* is the integral breadth of reciprocal lattice point, d^* is the lattice plane spacing, , $D_{H\text{-}W}$ is Halder-Wagner crystallite size, $\varepsilon_{H\text{-}W}$ is the lattice strain and K is the shape factor, which is equal to 0.9 for spherical grain formation.

$$\beta^* = \frac{\beta \cos\theta}{\lambda} \;\; ; d^* = \frac{2\sin\theta}{\lambda} \qquad (2)$$

β is the full width at half maximum (FWHM), λ is the X-ray wavelength (1.5406 Å) and θ is the Bragg angle of reflection for respective peaks under consideration. Considering the Gaussian component of β^*, which is solely due to size and strain effects alone, the above equation can be rewritten as:

$$\left(\frac{\beta}{\tan\theta}\right)^2 = \frac{K\lambda}{D_{H-W}} * \frac{\beta}{\tan\theta . \sin\theta} + 16\varepsilon_{H-W}^2 \qquad (3)$$

This equation is in accordance with the plot of a straight line equation with $K\lambda$ / $D_{H\text{-}W}$ as slope and $16\varepsilon_{H-W}^2$, the intercept, from which the size and strain could be estimated.

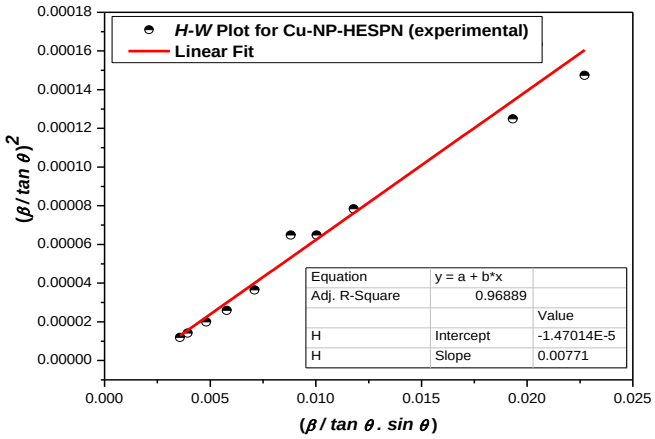

Fig. 3. Halder-Wagner plot of XRD data for Cu-NP-HESPN

Figure 3 represents, the Halder-Wagner (*H-W*) plot, from which the estimated crystallite size is found to be 18 nm and the negative value for strain implies that the adjacent crystallites get agglomerated themselves to form larger grains, which resulted the decreases in strain and hence reduces the surface energy of formation.

3.2. Morphological analysis

Field Emission Scanning Electron Microscope (FESEM) patterns recorded for Cu-NP-HESPN sample using Nova NanoSEM 450 device at various magnifications such as 2,00,000, 1,50,000, 1,00,000 and 50,000 are depicted in figure 4. It is apparent from the images that the sample is composed of uniform spherical gains with average diameter 55 nm. This spherical surface morphology is in well agreement with the shape factor used in Halder-Wagner analysis of XRD pattern. In our previous attempt [3] of synthesizing CuO nanostructures through the similar method which harnessed the chemical reduction of copper (II) sulfate pentahydrate using phytochemicals present in leaf extracts of *Leucas aspera*, the FESEM images clearly evidenced the formation of well dispersed long cylindrical rod shaped nanostructures along with a number of unshaped aggregates; unlike the spherical grains obtained here. This underlines that, the selection of phytochemical component along with other factors play a significant role in yielding the grains morphology.

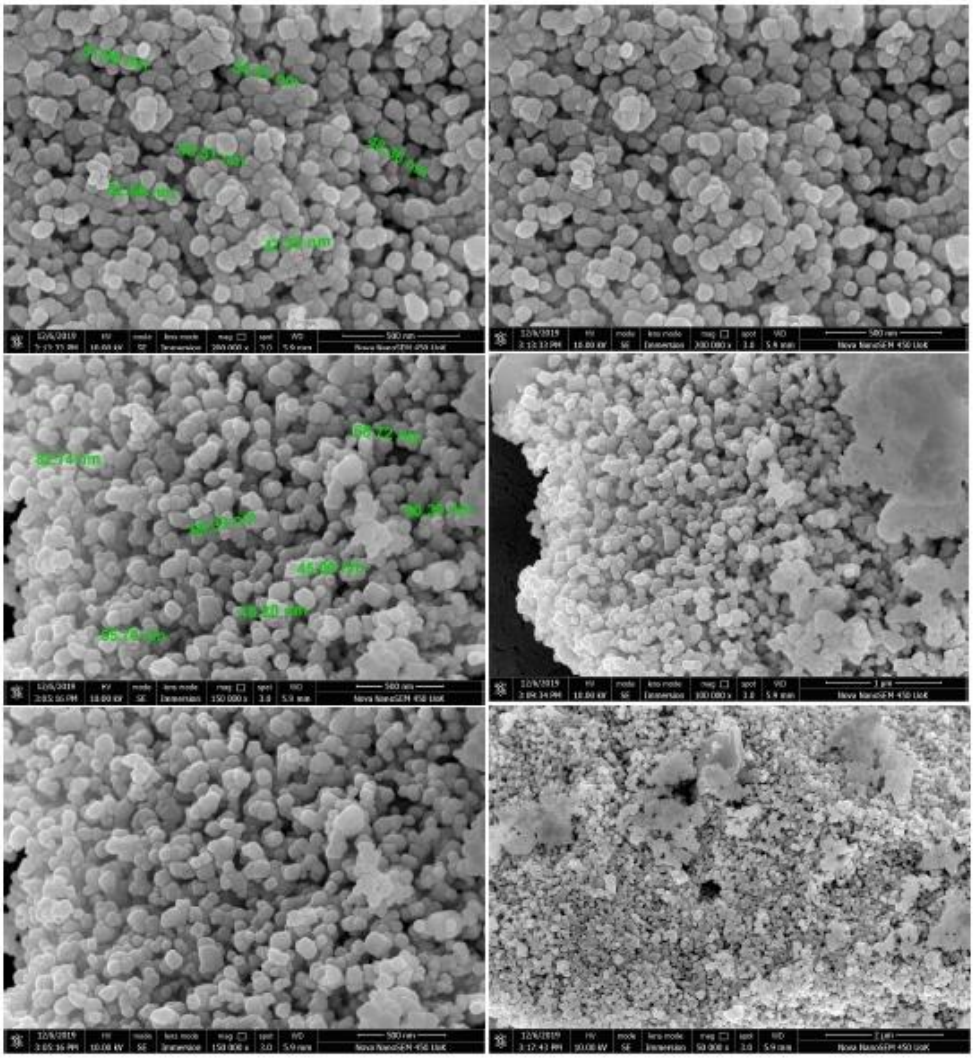

Fig. 4. FESEM images of Cu-NP-HESPN spherical grains at various magnifications

Further, it is evident that the Halder-Wagner crystallite size (18 nm), differ from the FESEM grain size (55 nm) in the sense that every three *H-W* crystallites in the Cu-NP-HESPN sample stabilizes by losing their surface energy through agglomeration and thus forming the FESEM spherical grains.

3.3. Estimation of band gap

The UV-visible spectrum for Cu-NP-HESPN sample recorded in reflection mode is depicted in figure 5; from which the band gap is estimated through Tauc's plot [17, 18] employing Kubelka-Munk equation [19].

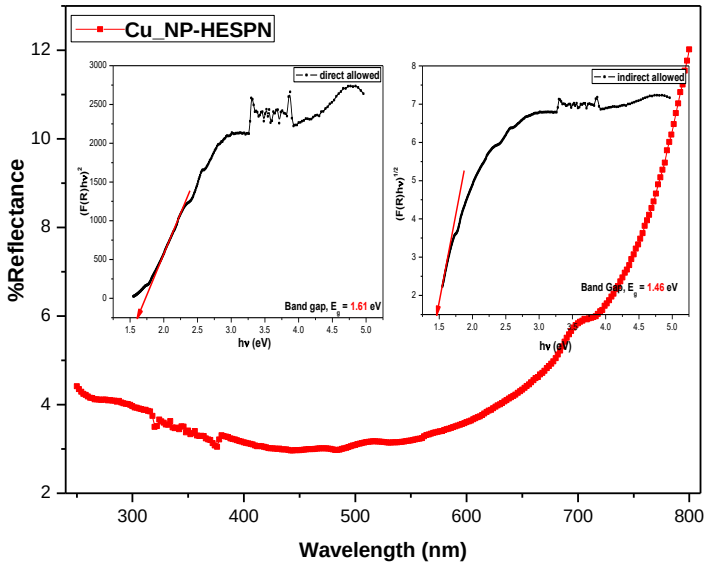

Fig. 5. UV-visible reflection spectrum recorded for Cu-NP-HESPN. The insets represent Tauc's plot corresponding to direct (n=1/2) and indirect (n=2) allowed transition modes.

Kubelka-Munk function [19] is calculated from the reflectance spectrum by the equation:

$$F(R_\alpha) = \frac{(1-R_\alpha)^2}{2R_\alpha} = \frac{k}{s} \qquad (4)$$

where $R_\alpha = R_{Sample} / R_{Standard}$ is the reflectance, k is the molar absorption coefficient and s is the scattering factor. From equation (4), it is apparent that $F(R_\alpha)$ is the relational function for absorption coefficient of the sample and hence a significant parameter in deciding the semiconducting efficacy, nature and band gap energy.

Further, the band gap can be estimated from the following actual relational expression employing Kubelka-Munk function, as proposed by Mott, Davis and Tauc [13, 17, 18, 20]:

$$F(R_\alpha)h\nu = A\,(h\nu - E_g)^n \qquad (5)$$

Where $h\nu$ is the photon energy, E_g is the optical energy gap situated between the localized states near the mobility edges according to the density of states model proposed by Mott and Davis [13, 20] and A is known as band tailing parameter which is independent of photon energy [21]. The constant (n) in equation (5) is known as the power factor of transition mode [13]. The value of power factor, say n = 2 stands for indirect allowed transition, n = 3 for indirect forbidden transition, n = 1/2 for direct allowed transition and n = 3/2 for direct forbidden transition [13].

In the case of perfectly crystalline semiconducting transition metal oxides, the direct band gap would be higher compared to indirect band gap [22]. Accordingly, the data have been plotted for both direct and indirect allowed transition modes. The insets of figure 5 shows the modified Tauc's plot employing Kubelka-Munk function corresponding to direct and indirect transition modes. The extrapolated linear portion of the curves to $F(R_\alpha) = 0$ provides

an estimation of optical direct band gap energy equal to 1.61 eV and indirect band gap energy to 1.46 eV. In agreement with XRD result, it is reasonable to infer that Cu-NP-HESPN sample consists of monoclinic end centered crystallites of CuO with optical direct band gap of 1.61 eV, as it could be evident that the one with best fit and higher value of band gap is corresponding to direct allowed transition mode. The value is still higher in comparison with monoclinic bulk copper (II) oxide, which is reported to have a narrow band gap of 1.2 eV [23]. The blue-shift behavior of optical band edge (increase of band energy) for this nanocrystalline CuO sample, in comparison with that of the bulk CuO is attributed to the enhancement of the quantum confinement effect [24]. Further, the band gap is direct in the sense that excited electrons in the lower levels of conduction band recombine radiatively with holes residing in the valence band at same momentum point [13], constituting an electron-hole pair, so called exciton, without the mediation of a third particle [13]. Here, the threshold for photon absorption and probably, the electron transport occurs through the same band edge [13] and hence may be considered as optical band gap or probably transport band gap [13].

3.4. Photoluminescence analysis

Figure 6 Photoluminescence (PL) spectrum of Cu-NP-HESPN was recorded with an optimized excitation wavelength of 280 nm. Figure 6 shows broad emission peaks centered on UV, violet far edge to blue-green edge visible regions. There are five peaks centered at 325 nm (3.82 eV), 381 nm (3.25 eV), 419 nm (2.96 eV), 465 nm (2.67 eV), 500 nm (2.48 eV). This fluorescence arises due to band to band transition in nanocrystalline copper oxide and other defect levels inside the nanoparticles. Corresponding to 280 nm excitation line, the highest intensified emission peak is observed at 381 nm [25]. The emission originates from the radiative recombination of electron-hole pair [25, 26]. Since the lamp was 280 nm UV, in order to avoid its harmonics to be emitted, the spectrum was restricted to a scan up to 530 nm.

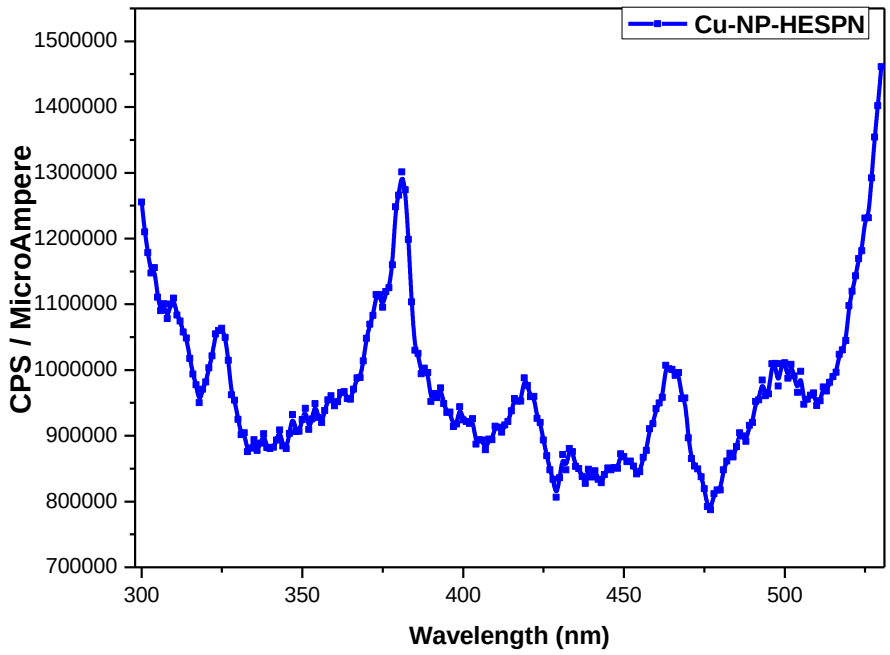

Fig. 6. PL spectrum recorded for Cu-NP-HESPN sample

Since the optical direct band gap obtained for Cu-NP-HESPN sample is 1.61 eV, all the said luminescence peaks could be attributed corresponding to band to band transition between the inner energy levels of copper oxide conduction and valence bands respectively.

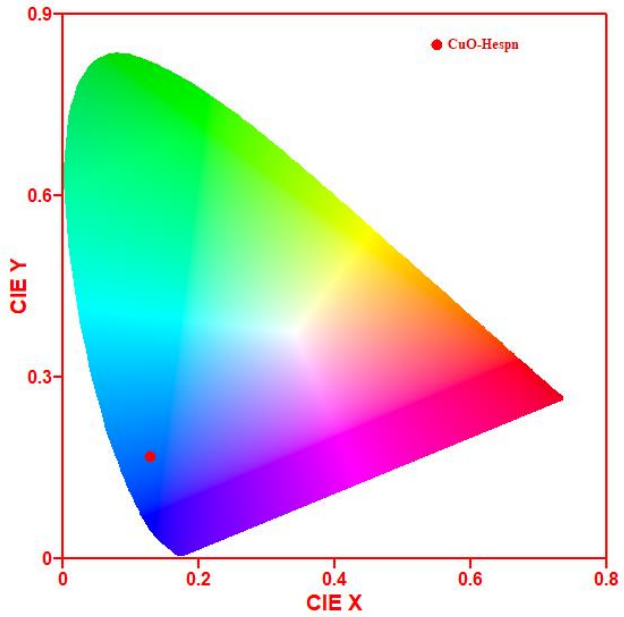

Fig. 7. CIE plot for Cu-NP-HESPN. The red spot in the blue region represents the calculated chromaticity coordinates

Further, figure 7 shows the Commission International de I'Eclairage (CIE) plot [27] of Cu-NP-HESPN sample. The average chromaticity coordinates [27] indicating the emission characteristics, calculated from the PL spectrum is found to be equal to (x = 0.131, y = 0.168) and is represented by the red spot in CIE plot, which falls in the blue region as shown in figure 7. This implies that in Cu-NP-HESPN sample, average emission occurs at the blue region of visible spectrum when excited using 280 nm UV source. Thus it is evident that, the prepared Cu-NP-HESPN sample is a potential candidate for blue display applications.

4. Conclusions

Monoclinic end centered phase of nanocrystalline copper (II) oxide (CuO) with *H-W* crystallite size 18 nm could be successfully synthesized using hesperidin mediated phytochemical reduction technique. The FESEM images clearly evidenced that the sample composed of uniform spherical grains in agreement with the shape factor used in Halder-Wagner analysis of XRD pattern. Tauc' plot corresponding UV-visible spectrum employing Kubelka-Munk function provided a direct optical band gap equal to 1.61 eV. The photoluminescence spectrum recorded using 280 nm optimal excitation wavelength and the calculated chromaticity coordinates revealed that the optical emission fall in the blue region of the CIE plot. Thus it is evident that, the prepared Cu-NP-HESPN sample is a potential candidate for blue display applications.

Acknowledgements

The authors are thankful to the authorities of Research and Postgraduate Department of Physics (Approved Research Center of University of Kerala), S.N. College, Kollam-691001, Kerala, India, for providing facilities to carry out the sample synthesis part of this research work. Also thanks are due to Department of Physics, Department of Optoelectronics and SICC at Kariyavattom Campus, University of Kerala, Thiruvananthapuram, Kerala, India for extending various facilities to perform characteristic measurements.

References

[1] H. Cavusoglu, R. Aydin, Superlattices and Microstructures, 128 (2019) 37-47.
[2] S. P. Kamble, V. D. Mote, Solid State Sciences, 95 (2019) Article 105936.
[3] Arun S. Prasad, Materials Science-Poland, 37(3) (2019). 503-509.

[4] Kavitha Pathakoti, Manjunath Manubolu, Huey Min Hwang Handbook of Nanomaterials for Industrial Applications: Micro and Nano Technologies, (2018) 894-907.
[5] M.Nasrollahzadeh, M.S.Sajadi, A.Rostamivartooni, J. Colloid Interface Sci., 459 (2015) 183-188.
[6] S.K. Li, Y.Y. Pan, M.Wu, F.Z. Huang, C.H. Li, Y.H.Shen, Appl. Surface Sci., 315 (2014) 169-177.
[7] J. Liu, D. Xue, Adv. Mater., 20 (2008), 2622-2627.
[8] G. Zhu, H. Xu, Y. Xiao, Y. Liu, A.Yuan, X.Shen, ACS Appl. Mater. Interfaces, 4(2012) 744-751.
[9] Jiang X., Herricks T., Xia Y., Nano Lett., 2 (2002) 1333-1338.
[10] S.Sonia, N. Jayram, S.P.Kumar, D.Mangalaraj, N. Ponpandian, C.Viswanathan, Super Latt. Microstruct., 66 (2014) 1-9.
[11] C.Y. ang, X. Su, F. Xiao, J. Jian, J. Wang, Sensor. Actuat. B, 158 (2011) 299-300
[12] S.K. Li, Y.Y. Pan, M. Wu, F.Z. Huang, C.H. Li, Y.H. Shen, Appl. Surface Sci., 315 (2014) 169-177.
[13] Arun S. Prasad, Mater. Sci. Semicond. Process., 71 (2017) 342-347.
[14] Mao-Qiang Man, Bin Yang, and Peter M. Elias, Evidence-Based Complementary and Alternative Medicine (2019), Article ID 2676307, 19 pages.
[15] B.D. Cullity, Elements of X-ray Diffraction, Addison-Weslev, Reading (1978).
[16] N. C. Halder, C. N. J. Wagner Advances in X-Ray Analysis (1966) 91-102.
[17] Tauc, R. Grigorovici, and A. Vancu,Phys. Status Solidi, 15 (1966) 627-637.
[18] J. Tauc (F. Abeles ed.), Optical Properties of Solids, North-Holland (1972).
[19] A. B. Murphy, Solar Energy Mater. Solar Cells, 91 (2007) 1326-1337.
[20] E. A. Davis and N. F. Mott, Philos. Mag., 22 (1970) 903-922.
[21] B. Tbib, M. Eddya, K. El-Hami. Phosphates based pigments for new anti-corrosion application: Synthesis and characterization, AIP Publishing, (2018).
[22] A. A. Radhakrishnan, B. B. Beena, Indian J. Adv. Chem. Sci., 2 (2014) 158-161.
[23] N. R. Dhineshbabu, V. Rajendran, N.Nithyavarthy, R.Vetumperumal, Appl. Nanosci. 6(2016) 933.
[24] A. El-Trass, H. ElShamy, I. El-Mehasseb, M. El-Kemary. Applied Surface Science, 258 (7) (2012) 2997-3001
[25] C. N. R Rao, F. L Deepak, Gautam Gundiah, A Govindaraj, Progress in Solid State Chemistry,31(1–2) (2003) 5-147.
[26] L.Xu , G.Zheng , S.Pei and J.Wang ,Optik 158 (2018) 382-390
[27] P.B. Devaraja,D.N. Avadhani, S. C. Prashantha, H. Nagabhushana, S.C. Sharma, B.M. Nagabhushana, H.P. Nagaswarupa, H.B. Premkumar, Spectrochim, Acta A Mol., Biomol, Spectrosc. 121(2014) 46-52.